Life Sciences 381 (2025) 123982

Contents lists available at ScienceDirect

Life Sciences

journal homepage: www.elsevier.com/locate/lifescie

Exposure to low-dose CuO nanoparticles improves fear extinction memory and enhance intrinsic excitability in the infralimbic cortex of male mice

Rahma Ammar [a,b], Laura E. Maglio [b], Mariem Naffeti [c], María Covadonga Aguado Ballano [b], Marta Callejo-Móstoles [b], Yassine Chtourou [a], Hamadi Fetoui [a], David Fernández de Sevilla [b,*]

[a] Laboratory of Toxicology-Microbiology and Environmental Health (17ES06), Faculty of Sciences of Sfax, University of Sfax, BP1171, 3000 Sfax, Tunisia
[b] Departamento de anatomía, histología y neurociencia, Facultad de Medicina, Universidad Autónoma de Madrid, Madrid, Spain
[c] Laboratory of Nanomaterials and Systems for Renewable Energies (LaNSER), Research and Technology Center of Energy, Techno-Park Borj-Cedria, Tunis, Tunisia

ARTICLE INFO

Keywords:
CuO-NPs
Synaptic plasticity
Excitability
Fear conditioning

ABSTRACT

Aims: Nanomaterials have gained considerable attention for diverse medical applications, particularly in neurology. Copper oxide nanoparticles (CuO-NPs) exhibit unique nanoscale properties that enable close interactions with neuronal cells, highlighting their potential as therapeutic agents for modulating synaptic plasticity and improving cognitive function. We aimed to investigate whether low-dose CuO-NPs can enhance fear extinction memory and increase intrinsic excitability in the infralimbic cortex (IL) of male mice.

Materials and methods: Adult male mice were subjected to fear conditioning using auditory cues paired with footshocks. Following the administration of a low dose of CuO-NPs, behavioral performance was assessed by measuring freezing responses during extinction. Whole-cell patch-clamp recordings were then performed on IL pyramidal neurons to evaluate intrinsic excitability and AMPA/NMDA ratio. Transmission electron microscopy (TEM) was applied after 2 and 24 h to assess the ability of CuO-NPs to reach the brain.

Key findings: We demonstrated via TEM that CuO-NPs efficiently cross the blood-brain barrier within 24 h' post-administration. Using cued fear conditioning, we subsequently found that a single intraperitoneal injection of CuO-NPs enhanced fear extinction memory, as evidenced by a significant reduction in freezing behavior compared to control animals. Patch-clamp analysis confirmed that CuO-NPs increased the excitability of IL pyramidal neurons and induced a sustained reduction in fast, medium, and slow post-spike after hyperpolarizations. Additionally, we demonstrated that CuO-NPs increased *N*-methyl-D-aspartate receptor-mediated synaptic currents, suggesting an enhanced synaptic plasticity in the infralimbic cortex.

Significance: Our findings offer new insights into the potential use of CuO-NPs for modulating fear extinction memory.

1. Introduction

Over the last decades nanotechnology has revolutionized modern medicine, providing innovative approaches to address persistent healthcare challenges [1]. Currently, around 100 nanomedicines have received approval from regulatory bodies such as the Food and Drug Administration (FDA) and European Medicines Agency (EMA), with over 500 more undergoing Phase I/II clinical trials [2]. In fact, nanoparticles (NPs) exhibit unique physicochemical properties distinct from conventional materials of the same composition which making them technologically valuable for diverse applications ranging from drug delivery and therapeutics to gene therapy, oncology and regenerative medicine [3]. Among the various types of nanoparticles studied, metal and metal oxide nanoparticles are especially noteworthy for their potential in drug delivery applications. In this context, copper oxide nanoparticles (CuO-NPs) have gained significant interest, especially for their biocompatibility and stability [4]. Additionally, CuO-NPs possess a defined size and shape that facilitates efficient crossing of the blood-brain barrier (BBB), which is typically a major obstacle for drugs targeting brain tissues. Previous studies demonstrated that Copper is an

* Corresponding author at: Department de Anatomy, Histology and Neuroscience, School of Medicine, Universidad Autónoma de Madrid, Spain.
E-mail addresses: ammar.rahma@outlook.fr (R. Ammar), lamaglio@ull.ed.es (L.E. Maglio), naffeti.mariam2@gmail.com (M. Naffeti), covadonga.aguado@uam.es (M. Covadonga Aguado Ballano), marta.callejo@uam.es (M. Callejo-Móstoles), yacine_chtourou@yahoo.fr (Y. Chtourou), hamadi.fetoui@fss.usf.tn (H. Fetoui), david.fernandezdesevilla@uam.es (D. Fernández de Sevilla).

https://doi.org/10.1016/j.lfs.2025.123982
Received 29 May 2025; Received in revised form 30 August 2025; Accepted 17 September 2025
Available online 22 September 2025

essential element that supports numerous neurological functions, especially those underpinning learning and memory. It serves as a cofactor for key enzymes involved in mitochondrial energy production [5], antioxidant defense (e.g., Cu/Zn superoxide dismutase) [6], and neurotransmitter synthesis, including the conversion of dopamine to norepinephrine [7]. Several mechanistic studies suggest that regulated copper levels can support synaptic function. For example, Gaier and al (2013) [8]demonstrated that physiological levels of copper can modulate neurotransmission by influencing synaptic proteins like PSD-95 and improving signaling at key neuronal junctions. Furthermore, dietary supplementation with a low dose of CuO-NPs has been found to enhance neuronal communication through an increase in the activity of acetylcholinesterase (AChE) and the expression of lipoprotein receptor-related protein 1 (LRP1) [9]. At the same time, CuO-NPs reduce the levels of *Tau* protein, amyloid (AP), glycosylated AChE (GAChE), and calcium/calmodulin-dependent protein kinase II alpha (CAMK2α) in the hippocampus [9,10]. Moreover, both in vitro and in vivo studies have shown that treatment with CuO-NPs in glioma-bearing rats reduced hippocampal inflammation, increased neurotransmitter release, and significantly enhanced spatial recognition and memory performance [11].

Fear conditioning is a well-established behavioral paradigm used to investigate learning and memory in various species, including zebrafish, rodents, and humans [12–14]. In recent years, it has also been increasingly applied to model human psychiatric conditions, offering valuable clinical insights [15]. Disorders most frequently examined are those in which fear processing is dysregulated, particularly post-traumatic stress disorder (PTSD) [16,17].

Fear conditioning represents an associative learning process where a neutral stimulus (conditioned stimulus [CS]; e.g., tone) acquires the capacity to evoke fear after being paired with an aversive stimulus (unconditioned stimulus [US]; e.g., electric shock). Fear extinction, an active inhibitory learning process, reduces conditioned fear responses through repeated CS exposure without US reinforcement [18]. Importantly, extinction doesn't erase the original CS-US association but creates a new inhibitory memory (CS-No US) that suppresses fear expression [19]. Both human and rodent studies demonstrate that fear extinction learning and memory depend on coordinated interactions among the amygdala, hippocampus, and infralimbic cortex (IL). The extinction memory involves long-term synaptic plasticity and increased excitability of pyramidal neurons (PNs) in the infralimbic cortex (IL). During extinction, the enhanced IL activity may inhibit fear by reducing activity output from the amygdala [20], a structure critical for learning and expressing fear memories [21]. In fact, IL neurons project to GABAergic intercalated (ITC) cells in the amygdala, creating a feedforward inhibitory circuit that suppresses central amygdala (CeA) output and prevents fear expression [22,23]. Importantly, impairments within the neural pathways responsible for fear processing contribute to the development of psychiatric disorders including phobias and PTSD [24]. Although previous studies [8,25–27] have shown that CuO nanoparticles can improve cognitive functions such as spatial learning and memory, their effects on fear-related learning particularly fear extinction remain unexplored. Given the emerging evidence that CuO-NPs can modulate neuronal function and cross the blood-brain barrier, we aimed to explore their potential role in facilitating fear extinction memory. This study aims to investigate the effects of low-dose CuO nanoparticles on the intrinsic excitability of IL neurons and their potential to facilitate fear extinction memory in rodents. We hypothesize that CuO nanoparticles, at low and safe concentrations, can enhance neuronal excitability in the IL cortex and promote more effective fear extinction. Our findings provide a first step toward understanding the neurobiological impact of CuO-NPs on fear-related learning and memory and open new avenues for their therapeutic application in anxiety and trauma-related disorders.

2. Materials and methods

2.1. Animals

Male adult mice aged 2 months old and weight 22.5 g were group-housed in transparent polyethylene cages. They were entrained to a 12:12 h light/ dark cycle with free access to food and water. All animal procedures were approved by the Universidad Autónoma of Madrid Ethical Committee on Animal Welfare and followed Spanish and European rules for the protection of experimental animals (Directive 2010/63/EU). An attempt was made to reduce the number of animals.

2.2. Preparation of nanoparticles (CuO-NPs)

Copper nanoparticles (CuO-NPs) used in this study are commercial particles (Sigma-Aldrich, Germany) synthesized as a powder. CuO-NPs (5 mg/kg) was prepared in Milli Q water and sonicated by Ultrasonic Sonicator Bath (J.P. SELECTA, Model 3000), at a frequency of 40 kHz and power of 50 W at 25 °C, for 30 min.

2.3. Characterization of nanoparticles (CuO-NPs)

A comprehensive array of characterization techniques was employed to analyse CuO-NPs. Scanning Electron Microscopy (SEM) images were generated using a Phillips XL30 device to characterize shape and size of nanoparticles. Energy Dispersive X-ray spectroscopy (EDX) was coupled with the SEM instrument to analyse the morphology and purity of CuO-NPs. X-ray diffraction (XRD) patterns were collected using an automated Bruker D8 advanced X-ray diffractometer with Cu Kα radiation ($\lambda = 1.54$ Å) for detailed crystallographic examination. Furthermore, Structural analysis was accomplished using Fourier-transform infrared (FTIR) spectroscopy (Model FTIR 6700, NICOLET) in attenuated total reflectance (ATR) mode.

2.4. Transmission electron microscopy (TEM) of medial prefrontal cortex

To assess the ability of copper oxide nanoparticles to reach the brain after 2 and 24 h, the medial prefrontal cortex was observed by TEM. First, the animals were intraperitoneally injected with MilliQ water or CuO-NPs (5 mg/kg). After 2 and 24 h, the mice were anesthetized with intraperitoneal injection of pentobarbital (30 mg/kg) and perfused through the heart with 50 mL PBS (137 mM NaCl, 2.7 mM KCl, 10 mM Na_2HPO_4, and 1.8 mM KH_2PO_4) followed by fixation using paraformaldehyde (4 %) and glutaraldehyde (1 %) in 0.1 M sodium cacodylate buffer. The brains were rapidly removed and immerged in the same solution at 4 °C for 24 h. Coronal slices were cut at a thickness of 40 μm with a vibratome (Leica VT 1200S) and incubated in osmium tetroxide (1 %) and potassium ferrocyanide (0.8 %) overnight at 4 °C. Samples were stained by with 2 % uranyl acetate, dehydrated via an ethanol gradient, and embedded them in epoxy resin. Subsequently, 2-mm^3 tissue of medial prefrontal cortex were carefully excised from coronal slices. Semi-thin sections (1 μm of thickness) stained with toluidine blue were examined by light microscopy to verify sample orientation and precise location (Infralimbic). For electron microscopy, ultra-thin sections (60 nm) were cut and placed onto copper slot grids. Finally, images were obtained using a Transmission Electron Microscope (JEOL jem 1010).

2.5. Cued fear conditioning

All behavioral experiments were conducted in two different white contexts (context A and context B) to minimize the impact of contextual associations. Context A was a rectangular chamber of 25 × 31 × 25 cm with transparent Plexiglas walls (Coulbourn, Allentown, PA) and a surface grid floor (26 parallel stainless-steel bars of 5 mm diameter and 6 mm spacing) connected to an electrical shocker. This context was

illuminated with a single overhead white light (28 V) and cleaned with a 70 % ethanol solution. Context B was a triangle chamber with smooth Plexiglas walls and floor, illuminated with two overhead white lamps, and cleaned with a 30 % coconut solution. These contexts were used separately and placed inside a sound-attenuating box (Med Associates, Burlingame, VT).

Animals were first housed and habituated to the experimenter and test environment by handling once a day for three consecutive days before fear conditioning training (10 min/day). On training days, mice were moved inside their home cage to a room next to the training room for 1 h before each test. Animals were transferred to context A (day 1) and fear-conditioned by five presentations of tone (conditioned stimuli (CS); 4 kHz, 30s, 80 dB) co-terminated with electric foot shocks (unconditioned stimulus (US); 0.7 mA, 1 s) with an inter-trial of 2 min. On extinction day (day 2), mice were intraperitoneally injected with 0.5 mL of Milli Q water or 5 mg/kg of CuO-NPs. After 2 h, they were transferred to context B to receive extinction learning, which consists of 30 presentations of CS (during 30s) with an inter-trial of 30s. On day 3, mice were exposed to 6 presentations of CS (during 30s) with an inter-trial of 30s in context B to test for extinction 24 h later. All behavioral tests are recorded with a digital video camera mounted on the top of each context, and freezing time was measured using the AnyMaze software 5.14 (Stoelting). Mice were considered frozen when there was a complete lack of motion for 2 s during the CS presentation.

2.6. Slice preparation

Immediately after the extinction on day 3, mice were deeply anesthetized with intraperitoneal injection of pentobarbital (30 mg/kg) and subjected to heart perfusion with ice-cold sucrose solution (in mM): 189 sucrose, 3 KCl, 1.62 NaH_2PO_4, 5 $MgSO_4$, 26 $NaHCO_3$, 10 glucose, and 0.09 $CaCl_2$. The pH was adjusted to 7.2–7.3. Animals were decapitated and brains were rapidly removed and immersed in ice-cold sucrose solution. Coronal slices were cut with a Vibratome (Leica VT 1200S) at a thickness of 400 μm. Slices were obtained using cold artificial cerebrospinal fluid (ACSF) containing (in mM): 124 NaCl, 2.69 KCl, 1.25 KH_2PO_4, 2 $MgSO_4$, 26 $NaHCO_3$, 2 $CaCl_2$, 10 glucose, 1 ascorbic acid, and 3 sodium pyruvate and bubbled with carbogen [95 % O2, 5 % CO2]. Next, prefrontal cortical slices were incubated for 45 min at room temperature (22–24 °C) in ACSF and then transferred to a submersion recording chamber fixed to an upright microscope stage (BX51WI; Olympus,Tokyo, Japan) and superfused at 2–3 ml/min with carbogen-bubbled ACSF at room temperature. Layer 5 pyramidal neurons (L5PNs) were observed using a microscope equipped with infrared differential interference contrast video (DIC) microscopy and a 40× water immersion objective.

2.7. Electrophysiological recordings

Whole-cell voltage-clamp and current-clamp recordings were conducted on the soma of L5PNs from the infralimbic cortex using path-clamp techniques. Patch pipettes with a resistance of 4–8 MΩ were filled with an internal solution containing (in mM): 130 $KMeSO_4$, 10 HEPES-K, 4 Na_2ATP, 0.3 Na_3GTP, 0.2 EGTA, 10 KCl (buffered to pH 7.2–7.3 with KOH). pH-adjusted to 7.2–7.3 with KOH (280 mOsm). The intracellular solution used for AMPA/NMDA ratio recordings contained (in mM): 115 $CsMeSO_4$; 20 CsCl; 10 HEPES; 2.5 $MgCl_2$; 4 ATP—Na_2; 0.4 GTP-Na_3; 10 Na-phosphocreatine, and 0.6 EGTA, with pH = 7.25 adjusted with CsOH. Recordings were performed using a Cornerstone PC-ONE amplifier (DAGAN, Minneapolis, MN), and pipettes were positioned with a mechanical micromanipulator (Narishige, Tokyo, Japan). The holding potential was regulated at −60 mV, and series resistance was compensated to approximately 80 %. Acceptance criteria for L5PNs recordings included a seal resistance exceeding 1 GΩ and a stable series resistance (10–20 MΩ) that did not change by more than 20 % during the experiment. Data obtained from the recordings were subjected to low-pass filtering at 3.0 kHz and sampled at a rate of 10.0 kHz through a Digidata 1440 (Molecular Devices). All recordings were performed at room temperature on male mice that had undergone extinction training on day 3.

2.8. Intrinsic excitability

First, the excitability of IL-L5PNs was examined by assessing the number of action potentials (spike frequency) generated in response to a series of prolonged (1 s) depolarizing current steps (ranging from −50 to 425 pA). The threshold for action potential voltage was determined as the initial point on the ascending phase of the spike where the change in voltage exceeded 50 mV/ms. The amplitude of the spike was calculated as the difference between the action potential voltage threshold and the peak voltage. Additionally, using Clampfit10 software (Axon Instruments), we determined the characteristics of the action potentials recorded from IL-L5PNs, including first sweep, ratio IH/Iq, resistance, capacity and event start time.

Next, we investigated the after hyperpolarizing potentials (AHPs) using two distinct pulse protocols in the current-clamp mode. The fast AHP (fAHP) was induced by a 10 ms depolarizing pulse and the medium and slow AHP (mAHP and sAHP, respectively) were evoked by an 800 ms depolarizing pulse. The fAHP and mAHP were quantified based on the peak amplitude of the afterhyperpolarization, whereas the sAHP was determined as the average membrane potential between 50 ms and 280 ms following the 800 ms pulse [28]. To record the currents underlying these potentials, we applied the same protocol in voltage-clamp mode. The membrane potential was held at −60 mV, and the cell was depolarized to 0 mV for 10 ms to measure the fIAHP at the peak of the currents. To analyse mIAHP and sIAHP, the cell was depolarized to 0 mV for 800 ms. The mIAHP was measured as the peak current amplitude, while the sIAHP was quantified as the amplitude of the curve, within 50–280 ms after the peak of the current.

2.9. AMPA and NMDA excitatory postsynaptic currents

Excitatory postsynaptic currents (EPSCs), consisting of both AMPA receptor (AMPAR)- and NMDA receptor (NMDAR)-mediated components in IL-L5PNs, were assessed in response to a bipolar stimulation using Pt/Ir concentric electrode (OP: 200 mm, IP: 50 mm; FHC), connected through two silver-chloride wires to a stimulator and a stimulus isolation unit (ISU-165 Cibertec). To measure AMPA and NMDA receptor-mediated currents, picrotoxin (50 μM) was added to the ACSF perfusion solution at least 10–15 min before recording to block GABA-mediated currents. Recordings were performed in voltage-clamp mode, with the membrane potential held at −80 mV to record AMPA component of the ESPCs and at +60 mV to measure the NMDA component of the EPSCs. Excitatory postsynaptic currents (EPSCs) were recorded at each potential until their amplitudes stabilized. Stimulation was applied at a frequency of 0.3 Hz, with the intensity and duration adjusted to produce AMPA currents in the range of 50–100 pA. Recordings began 30 min after establishing whole-cell configuration to allow Cs diffusion from the pipette into the cell, effectively blocking K+ channels.

The AMPA/NMDA ratio was determined by dividing the AMPAR-mediated EPSC amplitude, measured as the peak EPSC amplitude at a holding potential of −80 mV, by the NMDAR-mediated EPSC amplitude, measured at +60 mV, 70 ms after the after the stimulation artifact. For each cell, up to three ratios were recorded and averaged to generate a single value.

2.10. Data analysis

Conditioned fear was quantified by measuring the percentage of time subjects exhibited freezing behavior during a 30-s tone presentation. Freezing was defined as the absence of all movement except respiration [29]. The total freezing time was recorded and converted into a

percentage for analysis. Behavioral data analysis was performed using the AnyMaze software 5.14 (Stoelting). Electrophysiological data were analyzed with Clampex 11.2, curves were plotted using SigmaPlot 16, and transmission electron microscopy (TEM) images were analyzed using ImageJ 1.5.

All statistics were performed in Prism 9 (GraphPad) after checking data normality via the Kolmogorov–Smirnov test. Unpaired *t*-tests were used for two-group comparisons (normal distribution), and Two-way ANOVA with Bonferroni post-hoc tests were used for multiple comparisons. Data are presented as mean ± standard errors (mean ± SEM). The level of significance was set at $*p < 0.05$, $**p < 0.01$, $***p < 0.001$ between treated groups and controls.

3. Results

3.1. Characterization of CuO-NPs

The surface morphology of copper oxide nanoparticles (CuO-NPs) was meticulously examined using SEM analysis, with the resulting image displayed in Fig. 1A. The analysis revealed a dense coverage of nanoparticles across the entire surface, showcasing a diverse morphology that includes both spherical and rod-shaped particles. To quantify the particle sizes, ImageJ software was employed to analyse the SEM micrograph, resulting in histograms presented in Fig. 1B. The size distribution of the CuO-NPs spans from 8 nm to 185 nm, with an average particle size of around 51 nm, predominantly concentrated in the range of 20 ± 5 nm.

An elemental composition analysis was performed using Energy Dispersive X-ray Spectroscopy (EDX) to ascertain the elemental composition of the sample. The EDX spectra, presented in Fig. 1C, clearly confirm the presence of Cu and O elements, with atomic percentages of approximately 68.62 % and 31.38 %, respectively. A faint peak attributed to elemental carbon (C) was also detected; this is likely due to surface contamination from the environment or may have originated from the SEM equipment, a common issue that is difficult to completely eliminate during sample preparation, handling, and storage. Significantly, the absence of any additional peaks in the EDX spectrum indicate that the CuO nanoparticles exhibit a high level of purity. This purity is crucial for ensuring the reliability and consistency of the nanoparticles' properties, which are essential for their potential applications.

X-ray Diffraction (XRD) patterns of CuO-NPs are presented in Fig. 1D. Several distinct peaks were observed at 2θ values of 32.39° (110), 35.44° (002), 38.82° (111), 46.11° (−112), 48.70° (−202), 53.33° (020), 58.38° (202), 61.49° (−113), 66.14° (−311), 68.09° (220), 72.42° (311) and 75.17° (310) corresponding to various crystallographic planes of the monoclinic phase of CuO. These peaks were identified and matched with the reported standards from the Joint Committee on Powder Diffraction Standards (JCPDS) [30].

Notably, the prominent peaks at 2θ = 35.44° and 38.82° are characteristic of the pure monoclinic phase of CuO-NPs. The sharp and narrow diffraction peaks, coupled with the absence of additional peaks indicating secondary phases or impurities, confirm the high crystalline quality and purity of the material. This affirms that it is a single-phase structure consisting solely of the CuO phase, consistent with the EDX results.

In addition to providing insights into orientation and crystallinity, the XRD data allows for the calculation of the crystallite size (D) of CuO nanoparticles using the Debye-Scherrer formula, as outlined in Eq. 1 [30]:

$$D = \frac{k\lambda}{\beta\cos\theta} \quad (1)$$

where k is the Scherrer constant (approximately 0.9), λ is 0.154 nm, representing the wavelength of Cu-Kα X-ray radiation, β is the full width at half maximum (FWHM) of the XRD peaks, and θ is half of the Bragg angle.

The average nanoparticle size of approximately 26 nm was determined from the prominent diffraction peaks at (002) and (111). Remarkably, this estimation closely aligns with the values derived from SEM analysis, showcasing a predominant concentration of particles within the 20 to 30 nm range. This consistency reinforces the accuracy

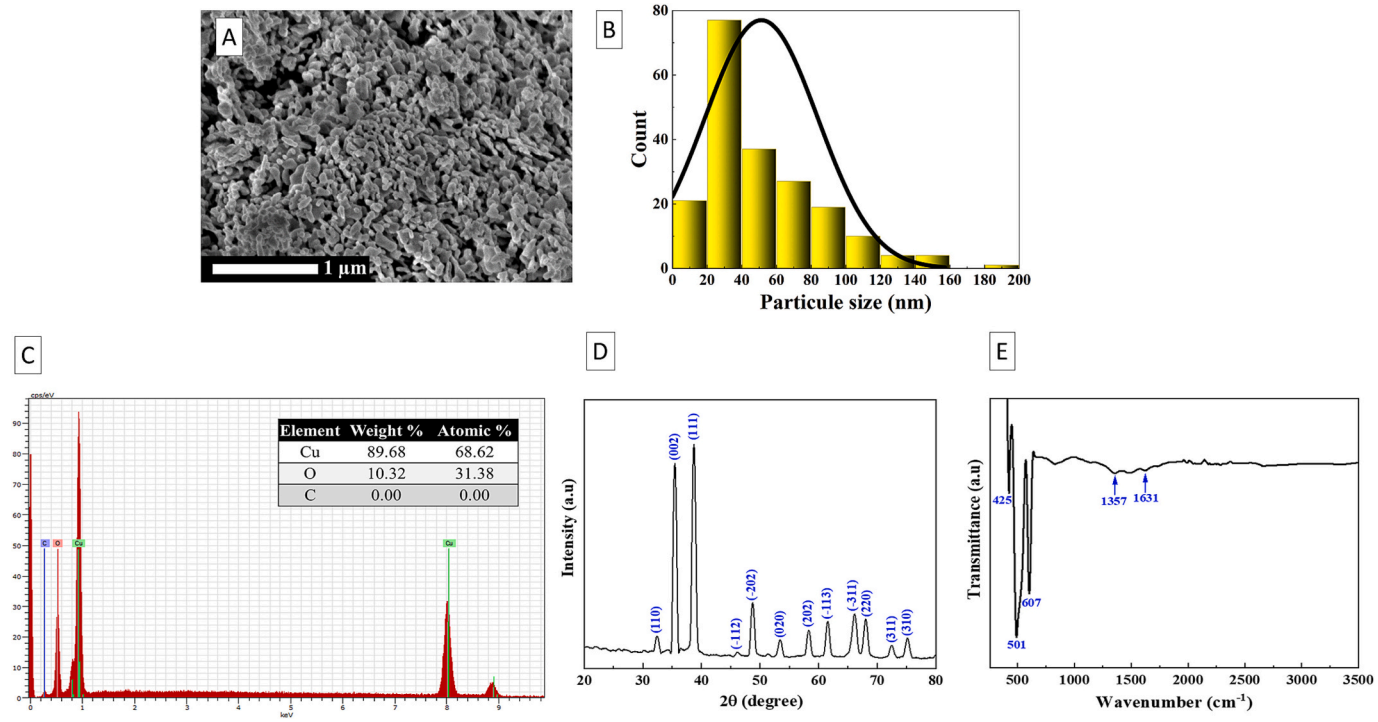

Fig. 1. Characterization of CuO-NPs in the powder. (A) Scanning Electron Microscopy (SEM) images; (B) CuO particle size distribution histogram; (C) EDX elemental analysis; (D) XRD pattern of CuO-NPs and (E) FTIR spectra of CuO-NPs.

and reliability of both measurement techniques.

FTIR analysis, a valuable tool for bond vibrational studies, was employed to analyse the CuO-NPs sample within the 400 cm^{-1}–3500 cm^{-1} range, as depicted in Fig. 1E. The peaks observed at 425 cm^{-1}, 501 cm^{-1}, and 607 cm^{-1} correspond to the characteristic Cu—O bond stretching vibrations of CuO [30]. Additionally, very faint broad bands at 1357 cm^{-1} and 1631 cm^{-1} were detected, attributed to C—H stretching vibrations and the presence of water molecules, respectively. The absence of vibrations in the range of 605–660 cm^{-1} effectively rules out the presence of other phases or impurities, such as Cu_2O. The FTIR analysis results are consistent with previous findings, further confirming the purity of the CuO-NPs.

3.2. Impact of CuO-NPs on ultrastructure of prefrontal cortex

To determine whether CuO-NPs reach the brain, the prefrontal cortex was analyzed using transmission electron microscopy (TEM). Prefrontal coronal slices were prepared from control mice and those injected intraperitoneally with CuO-NPs, specifically at 2 h and 24 h post-injection. Interestingly, TEM analysis revealed aggregated CuO-NPs within the vascular lumen associated with the blood-brain barrier (BBB) at 2 h post-injection. By 24 h, non-aggregated nanoparticles, approximately 6 nm in size, were observed within endothelial cells (Fig. 2). Importantly, no significant abnormalities in BBB ultrastructure were detected in the CuO-NP-treated groups compared to controls. Representative images showed capillaries with well-defined lumen surrounded by normal endothelial cells, typical mitochondria (Fig. 3D-F), and intact tight junctions, consistent across all groups (Fig. 2). Despite the presence of some cellular debris within the lumen in both control and treated samples, high-magnification views revealed endothelial vesicles in treated group after 24 h following the administration of CuO-NPs, potentially indicating transcytosis activity (Fig. 2C).

Ultrastructure examination of prefrontal cortex of treated animals did not exhibit distinguishable sign of death including apoptotic bodies, necrosis and autophagy (Fig. 3A-C). Additionally, cross-sectional pictures clearly showed the myelin sheath that surrounds axons. The overall structural appearance of myelin sheaths was comparable between control and treated brains, although variations in thickness were noted. Notably, pyramidal neurons located in deeper layers (V/VI) possess greater myelin coverage compared to those in superficial layers (II/III) (Fig. 3A-C) [31].

Furthermore, the examination of synaptic ultrastructure in the prefrontal cortex revealed no apparent abnormalities in treated mice compared to controls (Fig. 3G-I). To investigate synapse morphological property in a quantitative manner, the length and width of postsynaptic density (PSD), cleft width and synaptic vesicle diameter were measured by ImageJ software. Analysis of these parameters confirmed that CuO-NPs did not significantly alter synaptic morphology (Fig. 3J-M); Unpaired *t*-test).

3.3. CuO-NPs ameliorate fear extinction memory

To evaluate the effects of CuO-NPs on fear extinction memory, two groups of mice were examined: a control group ($n = 17$) receiving MilliQ water and a CuO-NP-treated group ($n = 18$) receiving 5 mg/kg CuO-NPs. Treatments were administered via intraperitoneal (IP) injection on Day 2, two hours before extinction training. On Day 1 (fear acquisition), both groups acquired similar freezing levels following five conditioning pairings (CS-US) (Fig. 4A; Control: 78 %; CuO-NPs: 78 %). During the extinction training session on Day 2 (30 CS presentations), both groups exhibited a comparable gradual reduction in freezing. However, during extinction Day 3, CuO-NP-treated mice displayed significantly lower freezing levels compared to controls (Fig. 4;A Control: 46.3 %; CuO-NPs: 10.2 %) indicating that CuO-NPs enhance extinction performance. To discriminate between an enhancement of recall of extinction and extinction learning, we averaged fear levels of the first two tones as a measure of recall of extinction, whereas the fear levels of 4 remaining tones were analyzed independently as a measure of extinction learning. CuO-NP-treated mice displayed similar freezing levels in the first two tones, whereas they showed an increasing significantly lower freezing levels to tones 3, 4, 5 and 6 (Fig. 4B), suggesting that CuO-NPs enhance extinction learning.

3.4. CuO-NPs modulate the excitability of IL-L5PNs

To investigate the effect of CuO-NPs on the excitability of IL-L5PNs during extinction memory facilitation, pyramidal neurones from both groups were recorded by whole-cell patch clamp immediately after the extinction on day 3. Neuronal excitability of IL-L5PNs was quantified by measuring the number of action potentials (APs) evoked by a series of

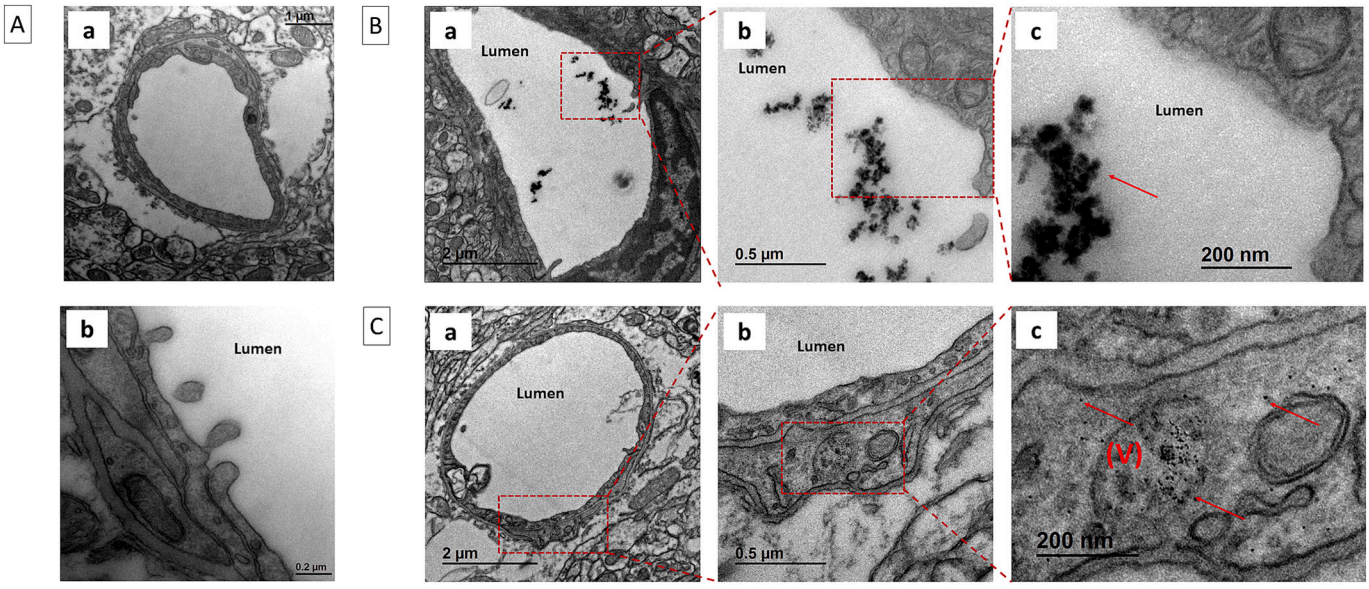

Fig. 2. TEM Images of mice prefrontal cortex Capillaries. (A) Control showing a normal blood-brain-barrier (BBB); (B) Capillary of CuO-NPs group 2 h following the administration of NP; (a) normal BBB with (a-c) the presence of aggregated CO-NPs in the lumen; (C) Capillary of CuO-NPs group 24 h following the administration of NP; (a-b) normal BBB with (c) the presence of CO-NPs in the endothelial cell. Red arrows indicate the CuO-NPs; (v) indicates vesicle.

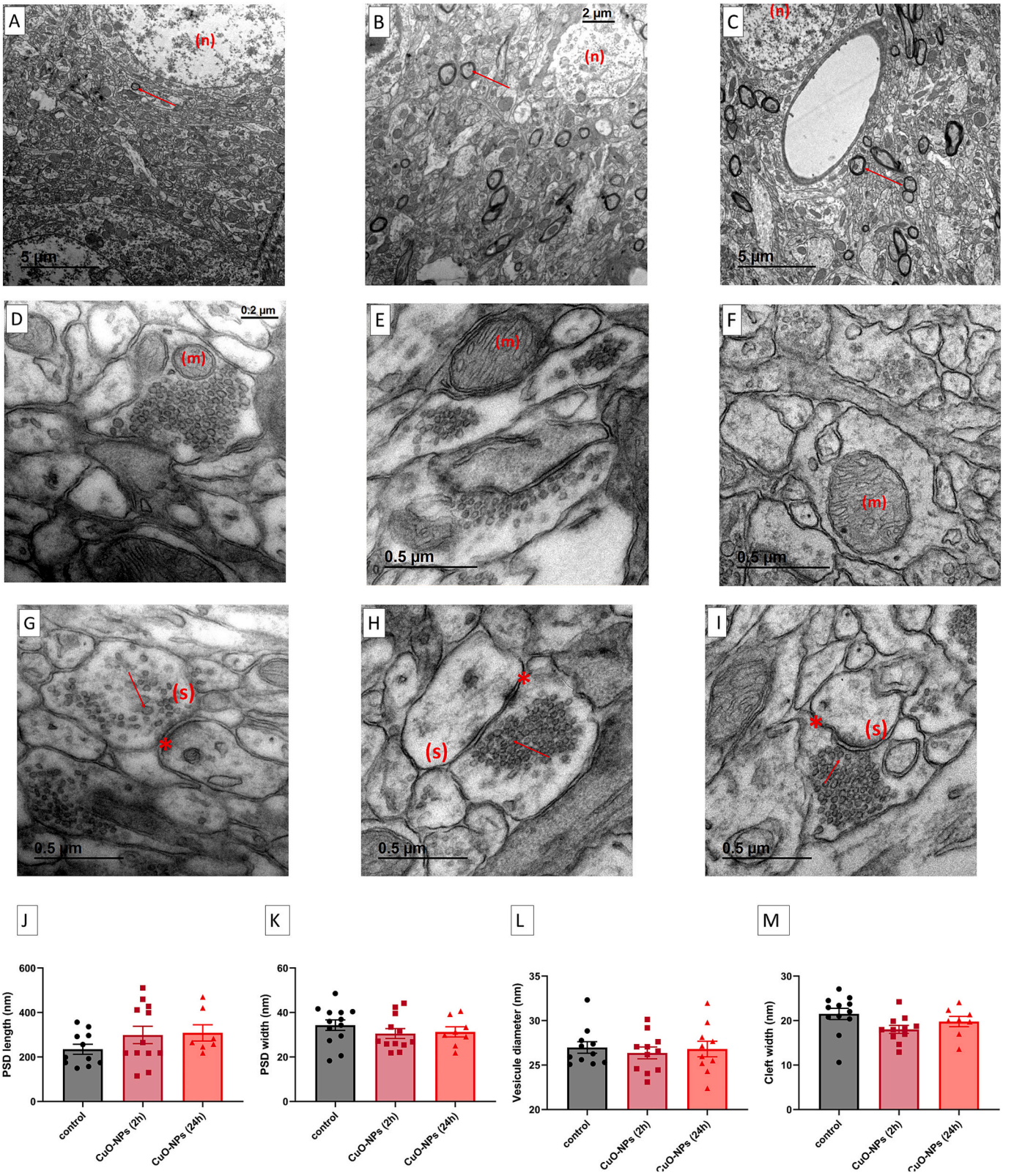

Fig. 3. Representative transmission electron micrographs (TEM) from (A, D, G) Control mice; (B, E, H) Mice 2 h after CuO-NP administration; and (C, F, I) Mice 24 h after CuO-NP administration. (A-C) Low-magnification images showing typical cortical ultrastructure, including neuronal nuclei (n) and myelinated axons (red arrows); (D—F) Higher magnification revealing normal-appearing mitochondria (m); (G-I) Synapses (s) appear structurally intact, with clearly visible presynaptic vesicles (red arrows) and synaptic clefts (red asterisks); (J-M) Quantification of synaptic morphology: Bar graphs showing (J) postsynaptic density (PSD) length, (K) PSD width, (L) synaptic vesicle diameter, and (M) synaptic cleft width ($n = 7$ images per group). Results are expressed as means ± SEM. *$p < 0.05$; **$p < 0.01$; ***$p < 0.001$; compared with controls, *t*-test.

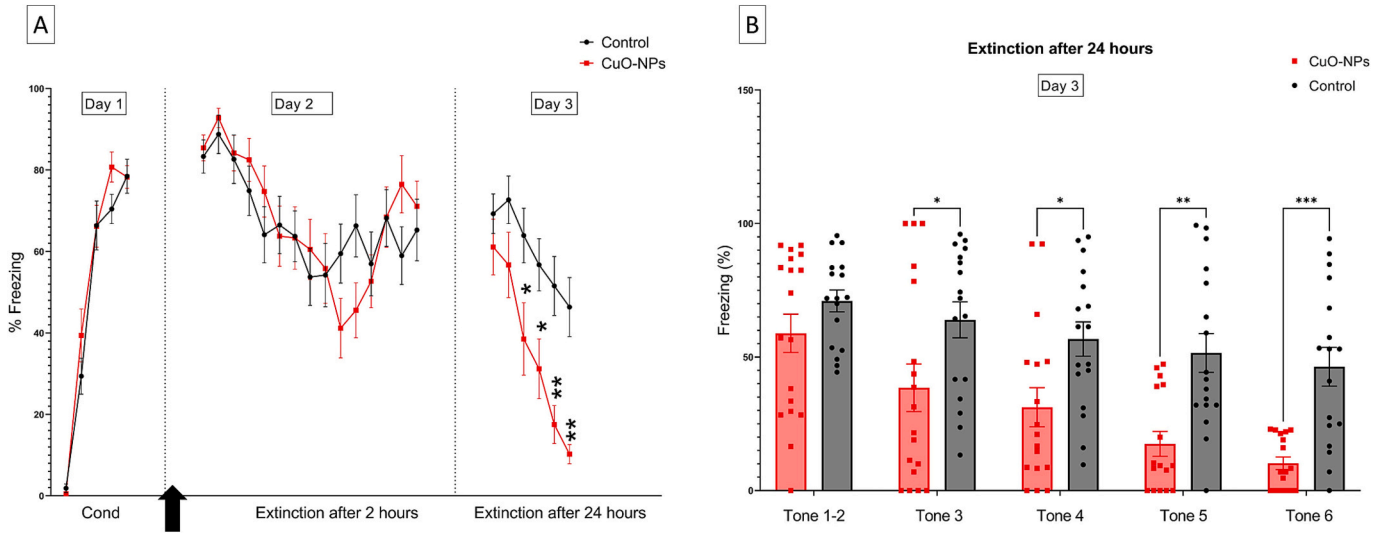

Fig. 4. CuO-NPs improve fear extinction. (A) Behavioral responses of groups. Control ($n = 17$) and CuO-NPs ($n = 18$) were intraperitoneally injected 2 h before extinction training (day 2) with milliQ and CuO-NPs respectively. The black arrow indicates the time of injection. In day 2 (extinction after 2 h of injection) each point in fear extinction represents the average of freezing level of two successive tones, whereas the freezing level to a single tone was represented in day1 (conditioning) and day3 (extinction after 24 h injection). (B) Bar diagram showing freezing behavior during extinction after 24 h of injection. The fear levels of the first two tones were averaged as a measure of recall of extinction, whereas the fear levels of 4 remaining tones were analyzed independently as a measure of extinction learning (*p < 0.05, **p < 0,01 MilliQ water vs Cu-ONPs; Two-way ANOVA followed by bonferroni multiple comparisons test).

depolarizing current pulses. In our study, neurons from CuO-NP-treated mice fired significantly more APs in response to current between 175 pA and 425 pA compared to neurons from control mice (Fig. 5), indicating increased firing frequency and thus neuronal excitability after CuO-NPs treatment. Other measured intrinsic physiological properties of IL-L5PNs were comparable between the two groups (Fig. 6).

3.5. CuO-NPs decrease the after-hyperpolarization properties in infralimbic neurones

Intrinsic excitability is modulated by different classes of potassium channels that underlie the fast, medium and slow after-hyperpolarization [32]. For this purpose, we measured the $_{f}$AHP and $_{f}I_{AHP}$ evoked by 10 ms depolarizing pulse in current and voltage clamp mode respectively. Interestingly, we observed a significant reduction in $_{f}$AHP and $_{f}I_{AHP}$ in neurons from the CuO-NPs group compared to the control group (Unpaired *t*-test, F = 1.051, $p < 0.01$; F = 1.606, $p < 0.05$ respectively; Fig. 7A-D). To confirm these results, we measured also the $_{m}$AHP and $_{s}$AHP evoked by 800 ms depolarizing pulse in current clamp mode. Recordings of IL-L5PNs showed a significant decrease of both mAHP and sAHP peak amplitudes in CuO-NPs group compared with control group (Unpaired *t*-test, F = 1.859, F = 1.503 respectively, $p < 0.05$, Fig. 7E-G). Moreover, we quantified $_{m}I_{AHP}$ and $_{s}I_{AHP}$ by depolarizing IL-L5PNs to 0 mV for 800 ms in voltage clamp mode. Importantly, our results revealed that both currents amplitude of CuO-NPs group were significantly smaller than those of the control group (Unpaired *t*-test, F = 1.194, F = 2.169 respectively, $p < 0.05$, Fig. 7H-J).

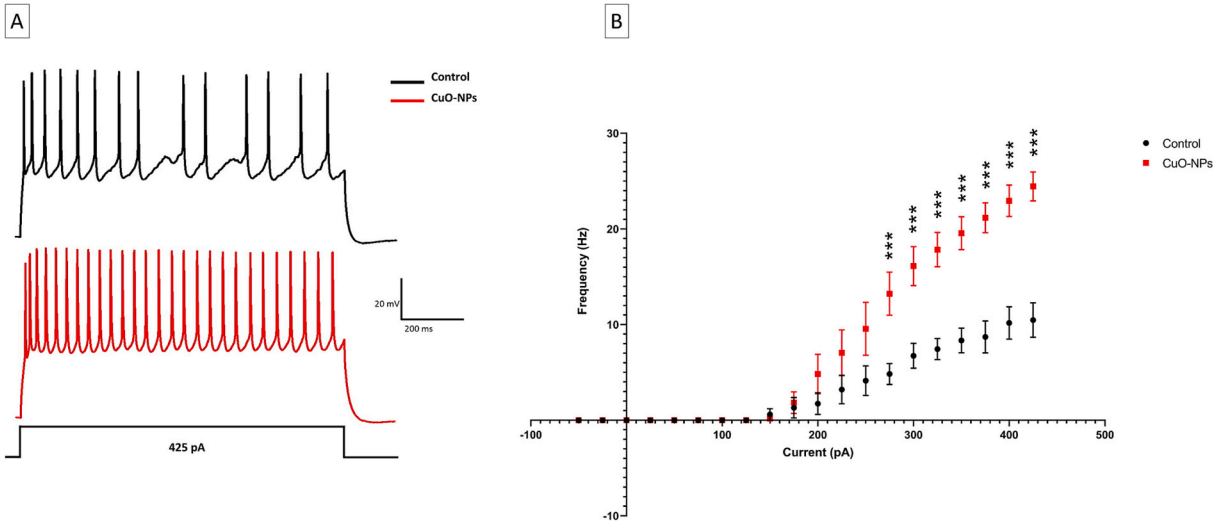

Fig. 5. CuO-NPs increase the excitability of L5PNs. (A) Representative traces recorded from IL- L5PNs after 425 nA current injection in control group (black) and CuO-NPs group (red); (B) Plot representing the frequency of APs in response to injected current (pA) for IL-L5PNs in control (black, $n = 5$ animals) and CuO-NPs (red, n = 5 animals). (***p < 0.001 control vs CuO-NPs; Two-way ANOVA followed by bonferroni multiple comparisons test).

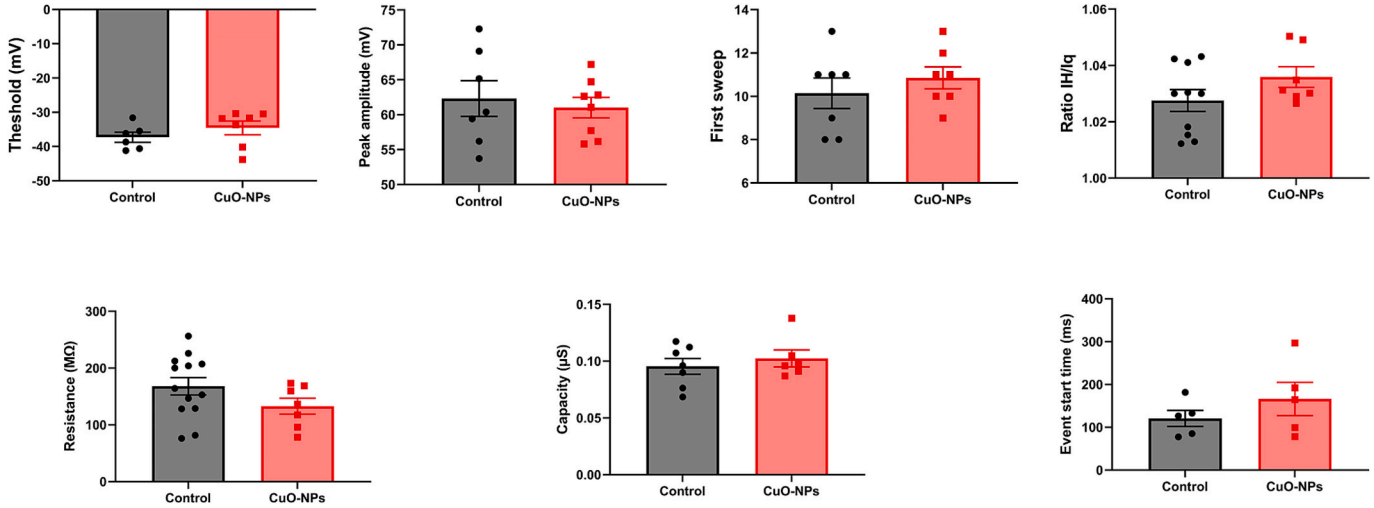

Fig. 6. Properties of action potential (AP).

3.6. CuO-NPs increase NMDAR-mediated EPSCs in IL-L5PNs

To investigate whether CuO-NPs induces synaptic changes in in IL-L5PNs, AMPAR- and NMDAR- mediated excitatory postsynaptic currents (EPSCs) were evoked by local extracellular stimulation. To block GABA -mediated inhibitory currents, picrotoxin was added to the bath solution. In this experiment, we used an intracellular solution that contained Cs^{+2} to block various potassium and sodium channels, thus reducing the effects of input resistance on EPSC measurements. Analysis of the electrophysiological recordings revealed a significant decrease of AMPA to NMDA ratios of neurons from CuO-NPs group compared with control group (Unpaired t-test, $F = 3.822$, $p < 0.05$; Fig. 8A-B). To evaluate whether changes in AMPA to NMDA ratios were due to changes in AMPAR- or NMDAR-mediated EPSCs, we analyzed each component separately in IL-L5PNs. First, we examined the AMPA component and found no significant differences in AMPAR EPSCs across groups (Unpaired t-test, $F = 1.411$, $p < 0.05$; Fig. 8C). Interestingly, we observed a significant increase in NMDAR- mediated EPSCs in CuO-NPs group compared with the control (Unpaired t-test, $F = 2.979$, $p < 0.05$; Fig. 8D). These findings suggest that the observed changes in AMPA to NMDA ratios were mainly due to the increases in NMDAR-mediated synaptic activity.

4. Discussion

Copper oxide nanoparticles (CuO-NPs) have emerged as a promising tool in neuroscience, offering innovative approaches treating neurological disorders and enhancing cognitive function [33,34]. While the neuroprotective effects of low-dose CuO-NPs on the hippocampus [9,10] and their ability to improve learning and memory [35] have been previously studied, their potential role in fear extinction memory and its mechanism remains unexplored. For the first time, our study demonstrated that a single intraperitoneal injection of CuO-NPs (5 mg/kg) enhances the fear extinction learning and memory in the infralimbic cortex (IL) through the increase of neuronal excitability and synaptic plasticity. While our study focused on the infralimbic cortex (IL) due to its critical role in fear extinction, it is important to consider that CuO-NPs may also exert effects in other brain regions. The presence of CuO-NPs in the prefrontal cortex was confirmed by our ultrastructural data; however, their distribution and impact in other fear-related areas, such as the amygdala or hippocampus, were not assessed. The apparent specificity to IL may reflect the timing of our recordings and the functional relevance of this region during extinction. Studying whether CuO-NPs influence neuronal activity and plasticity in these additional regions will bring additional evidence to better understand their broader neurobiological effects. Our electrophysiological findings in IL pyramidal neurons, specifically the enhancement of NMDAR-mediated currents and reduction in AHPs, are consistent with mechanisms known to facilitate IL-driven inhibition of amygdala output via intercalated cells. CuO-NPs may modulate infralimbic cortex activity in a way that indirectly influences amygdala function, although we did not directly assess amygdala activity in this study. Future studies should include direct recordings or imaging of amygdala activity to establish a more explicit link between CuO-NP-induced cellular changes and behavioral outcomes.

It is of relevance that CuO-NPs used in our experiment have different shape and size, as reported by scanning Electron Microscope (SEM). Transmission Electron Microscopy (TEM) analyses of prefrontal cortex tissues revealed the presence of aggregated CuO-NPs in the lumen of the blood brain barrier (BBB) after 2 h of the administration of nanoparticle. Notably, the smaller particles tend to aggregate into larger clusters, a phenomenon likely attributed to van der Waals attraction forces [36]. Additionally, ultrastructural analysis of BBB provides evidence for the presence of non-aggregated nanoparticles, approximately 6 ± 2 nm in size, within endothelial cells after 24 h. It has been reported that smaller particles exhibit greater mobility than larger ones and are expected to traverse the BBB through carrier-mediated endocytosis or passive diffusion [37,38]. Interestingly, the ultrastructure of prefrontal cortex did not exhibit any significant abnormalities or distinguishable sign of death, suggesting the biocompatibility of CuO-NPs. Our results are in line with previous in vivo and in vitro studies demonstrating that a low dose of CuO-NPs or other small inorganic nanoparticles and nanoobjects cross effectively the BBB without damaging the ultrastructure of the brain [35,39–41]. These unique physical and chemical properties of CuO-NPs used in the present study may enhance their potential application in extinction of conditioned fear memory. In the present study, we intraperitoneally injected CuO-NPs two hours before the extinction protocol and found that they did not affect fear extinction at that time point. However, 24 h later, the CuO-NPs significantly enhanced fear extinction memory as assessed by a faster decline in freezing during extinction relative to the control group. These results align with ultrastructural analysis of the BBB, which showed that CuO-NPs were unable to reach the brain after 2 h but successfully crossed the BBB after 24 h. Importantly, our biodistribution data indicate that CuO-NPs are not detectable in the brain 2 h post-injection, but are present at 24 h, suggesting a delayed crossing of the blood-brain barrier. This supports the interpretation that CuO-NPs did not influence extinction on Day 2, but their presence in the brain by Day 3 raises the possibility that they may have affected the extinction occurring this day. Moreover, it is plausible that the observed effects on day three reflect enhanced extinction

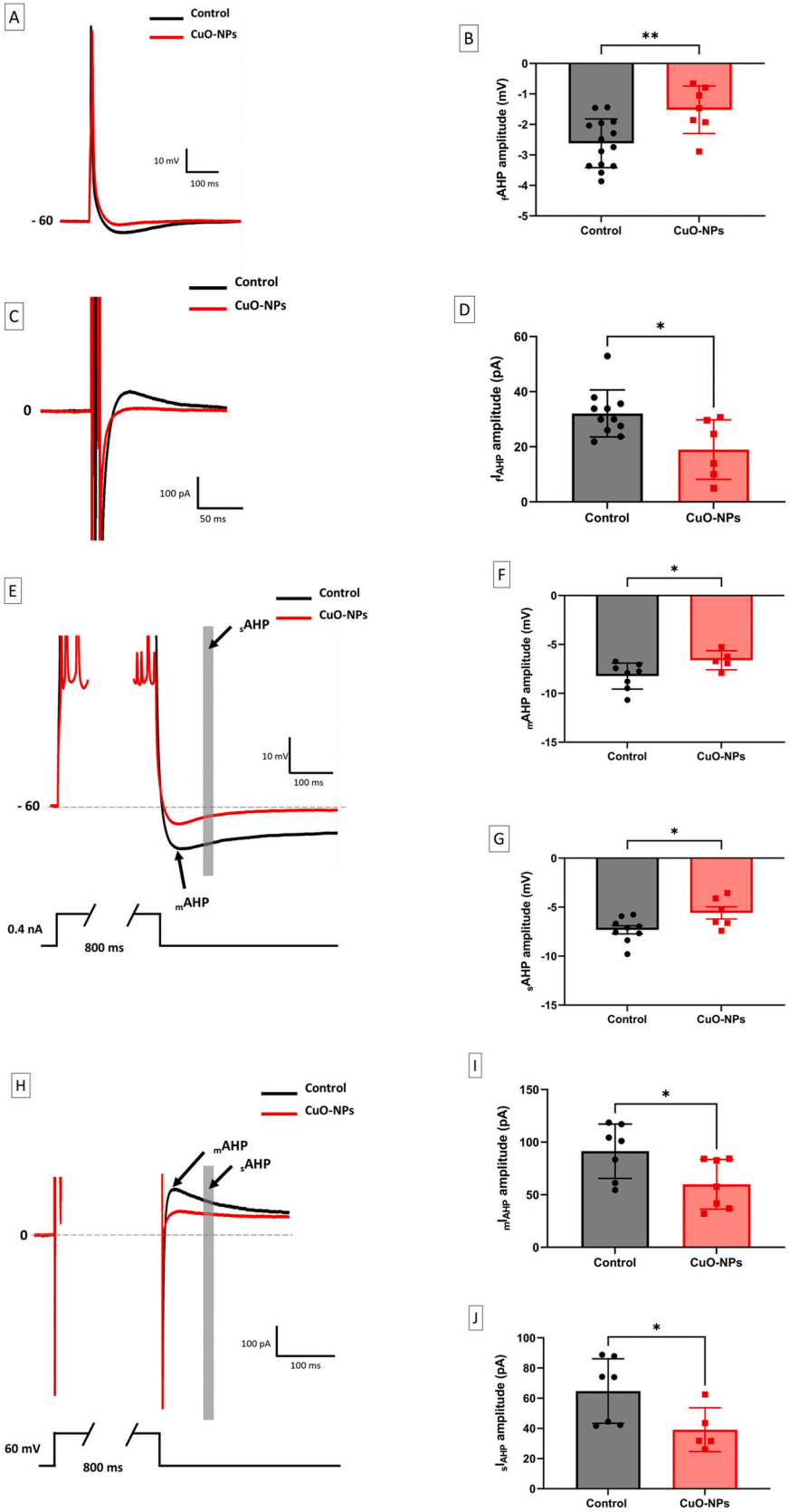

(caption on next page)

Fig. 7. CuO-NPs decrease AHP in L5PNs. (A) Superimposed average traces of the fAHP recorded in control group (black) and CuO-NPs group (red) after the extinction on day 3; (B) Peak amplitude of the fAHP; (C) Superimposed current traces recorded from IL-L5PNs of control group (black) and CuO-NPs group (red) in response to a 10 ms depolarizing voltage pulse from -60 mV to 0 mV; (D) Peak amplitude of the fIAHP; (E) Representative recordings from IL-L5PNs of hyperpolarizing potentials evoked by an 800 ms depolarizing pulse to study medium and slow AHP of the control group (black) and CuO-NPs group (red); (F and G) Bar diagram showing the peak amplitude of the mAHP and sAHP respectively; (H) Superimposed current traces recorded from IL-L5PNs of control group (black) and CuO-NPs group (red) in response to a 800 ms depolarizing voltage pulse from -60 mV to 0 mV to study mIAHP and sIAHP; (I and J) Bar diagram showing the peak amplitude of the mIAHP and sIAHP respectively. Results are expressed as means ± SEM. *p < 0.05; **p < 0.01; ***p < 0.001; compared with controls, t-test.

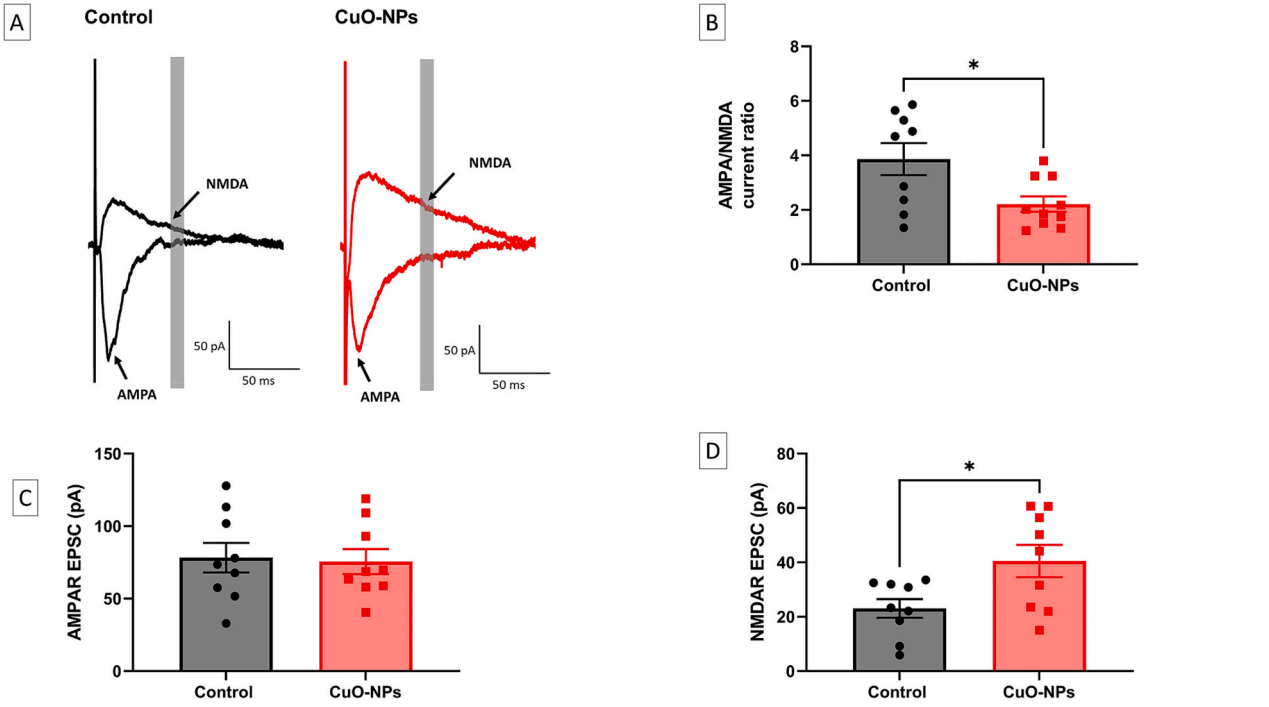

Fig. 8. CuO-NPs decrease AMPA/NMDA ratio in L5PNs. (A) Representative recordings of AMPAR- and NMDAR- mediated EPSC recorded at −60 mV and + 60 mV respectively for control group (black) and CuO-NPs group (red); (B - D) Bar diagram showing AMPA/NMDA ratio, AMPAR EPSC and NMDAR EPSC respectively. Results are expressed as means ± SEM. *p < 0.05; **p < 0.01; ***p < 0.001; compared with controls, t-test.

learning rather than pure recall. To discriminate between enhancement of learning vs recall of extinction, we analyzed the freezing behavior during the first two tone presentations on day three. This analysis revealed a significant difference between groups only in the last 4 tones, suggesting that CuO-NPs enhance extinction learning.

Indeed, extinction of cued-fear conditioning is an active learning process that is highly associated with increased excitability of pyramidal neurons (PNs) in the infralimbic cortex (IL) [42]. In order to get a clear perception of the effect of CuO-NPs administration on neuronal excitability in the IL, we used whole patch-clamp to evaluate their properties. Consistent with our recordings, CuO-NPs did not affect the AP characteristics, however, the excitability increased in IL-L5PNs from treated mice where the extinction was improved. Optogenetic [43], pharmacological [44,45] and electrophysiological [38] studies provide evidence that the increase in neuronal excitability is observed as a decrease in spike frequency adaptation during prolonged depolarizing current stimuli, caused by a reduction in post-burst afterhyperpolarization (AHP). Thus, intrinsic neuronal excitability, a form of non-synaptic cellular plasticity, supports learning and memory by modulating spike frequency adaptation and AHP [46–48]. Interestingly, AHP is mediated by different ion channels depending on its temporal characteristics [49]. Big-conductance Ca^{2+}-activated K^+ channels (BK channels) are implicated in generating the fast afterhyperpolarization (AHP) [50]. In contrast, the medium AHP is influenced by multiple currents, including small-conductance Ca^{2+}-activated K^+ channels (SK channels) [51], the hyperpolarization-activated current (I_h), and the M current [50,52]. However, the specific K^+ current responsible for the slow AHP remains unidentified [49]. In the present study, we observed that exposure to copper oxide nanoparticles (CuO-NPs) led to a long-lasting reduction in the fast, medium, and slow afterhyperpolarization (fAHP, mAHP, and sAHP) currents in IL-L5PNs of treated mice. This reduction in AHP currents was closely associated with the consolidation of fear extinction memory, indicating that CuO-NPs may exert their effects by modulating the ion channels responsible for generating these currents in IL-L5PNs. Similar to our findings, in vitro studies demonstrated that non-toxic dose (20 μg mL-1) of silica nanoparticles (50 nm-SiO2NPs) interact with plasmic membrane of GT1–7 neuroendocrine cells and increase firing frequency, without altering functional behavior over a time scale of hours. Additionally, incubation with these nanoparticles for up to 24 h did not result in any significant changes in gene expression [39,53].

Fear extinction is strengthened by enhanced NMDA receptor-dependent activity in IL, a critical process for memory consolidation [34,54]. An optogenetic study indicated that NMDAR currents at ventral hippocampal (vHC) synapses in IL are dynamically modulated by fear learning and extinction. Notably, fear conditioning weakened these currents, whereas extinction strengthened them without changing AMPAR currents [55,56] demonstrated that blocking NMDA receptors in the ventromedial prefrontal cortex (vmPFC) using the antagonist 3-(2-Carboxypiperazin-4-yl) propyl-1-phosphonic acid (CPP), either just before or immediately following extinction training, disrupts the recall of that extinction memory 24 h later. This suggests that extinction learning and memory relies on the activation of NMDARs within the vmPFC after the training occurs. Furthermore, electrophysiological studies demonstrated that NMDARs antagonists diminishes burst firing

in vmPFC neurons, implying that this bursting activity is crucial for successful extinction consolidation [57]. Additionally, recent investigation demonstrated that inhibiting SK potassium channels led to an increase in NMDAR function and facilitated long term potentiation (LTP) [58]. In this study, we used electrical stimulation of IL-L6 and found that a single intraperitoneal injection of CuO-NPs induced plasticity leading to an enhancement of NMDAR-mediated current and a corresponding reduction of AMPA/NMDA ratio. Although we observed synaptic changes consistent with enhanced plasticity, we did not perform direct LTP induction protocols in the infralimbic cortex. Our findings suggest that CuO-NPs enhance the impact of IL projections on downstream targets, particularly by boosting their activation of inhibitory intercalated cells in the amygdala, leading to reduced fear expression. It remains an open question whether CuO nanoparticles enhance learning in general or exert specific effects on fear extinction. In our study, CuO-NPs were administered prior to extinction training, and the observed behavioral and electrophysiological changes were interpreted in the context of extinction memory. However, it is possible that CuO-NPs could also modulate other forms of learning, including fear acquisition or spatial memory, depending on the timing and context of administration. Previous studies have suggested cognitive-enhancing effects of CuO-NPs, but their role in associative fear learning has not been directly tested. Future studies should explore whether CuO-NPs influence general learning mechanisms or act preferentially on extinction-related circuits.

In summary, this study provides new evidence that CuO-NPs enhances the intrinsic excitability of L5PNs of IL by reducing after-hyperpolarization currents (fIAHP mIAHP and sIAHP), and modulates NMDAR-mediated current, leading to a long-lasting increase in synaptic strength. Together, these forms of intrinsic and synaptic plasticity regulate neuronal connectivity in a way that facilitates the consolidation of fear extinction memory.

Acknowledgement section, sources of funding

This research was supported by grants PID2020-119358GB-I00 and PID2023-148843NB-I00 from the European Union (Ministerio de Ciencia e Innovacion and Ministerio Ciencia, Innovacion y Universidades, AEI/FEDER, UE) to David Fernández de Sevilla and the APC was funded by the CRUE-CSIC agreement with Elsevier.

CRediT authorship contribution statement

Rahma Ammar: Writing – original draft, Methodology, Formal analysis, Conceptualization. **Laura E. Maglio:** Writing – review & editing, Methodology, Formal analysis, Data curation. **Mariem Naffeti:** Writing – review & editing, Methodology, Data curation. **María Covadonga Aguado Ballano:** Writing – review & editing, Methodology, Formal analysis, Data curation. **Marta Callejo-Móstoles:** Writing – review & editing, Formal analysis, Data curation. **Yassine Chtourou:** Writing – review & editing, Supervision. **Hamadi Fetoui:** Writing – review & editing, Writing – original draft, Validation, Methodology, Formal analysis, Conceptualization. **David Fernández de Sevilla:** Writing – review & editing, Writing – original draft, Visualization, Methodology, Funding acquisition, Conceptualization.

Consent for publication

All authors give consent for the publication of the manuscript in Life Sciences.

Declaration of competing interest

The authors declare that they have no competing interests.

Data availability

Data will be made available on request.

References

[1] X. Ma, Y. Tian, R. Yang, H. Wang, L.W. Allahou, J. Chang, G. Williams, J. C. Knowles, A. Poma, Nanotechnology in healthcare, and its safety and environmental risks, J. Nanobiotechnol. 22 (2024) 715, https://doi.org/10.1186/s12951-024-02901-x.
[2] M.J. Woźniak-Budych, K. Staszak, M. Staszak, Copper and copper-based nanoparticles in medicine—perspectives and challenges, Molecules 28 (2023) 6687, https://doi.org/10.3390/molecules28186687.
[3] E. Karahmet Sher, M. Alebić, M. Marković Boras, E. Boškailo, E. Karahmet Farhat, A. Karahmet, B. Pavlović, F. Sher, L. Lekić, Nanotechnology in medicine revolutionizing drug delivery for cancer and viral infection treatments, Int. J. Pharm. 660 (2024) 124345, https://doi.org/10.1016/j.ijpharm.2024.124345.
[4] M. Devaraji, P.V. Thanikachalam, K. Elumalai, The potential of copper oxide nanoparticles in nanomedicine: a comprehensive review, Biotechnol. Notes 5 (2024) 80–99, https://doi.org/10.1016/j.biotno.2024.06.001.
[5] I.F. Scheiber, J.F.B. Mercer, R. Dringen, Metabolism and functions of copper in brain, Prog. Neurobiol. 116 (2014) 33–57, https://doi.org/10.1016/j.pneurobio.2014.01.002.
[6] J. Gale, E. Aizenman, The physiological and pathophysiological roles of copper in the nervous system, Eur. J. Neurosci. 60 (2024) 3505–3543, https://doi.org/10.1111/ejn.16370.
[7] J.R. Prohaska, A.A. Gybina, Intracellular copper transport in mammals, J. Nutr. 134 (2004) 1003–1006, https://doi.org/10.1093/jn/134.5.1003.
[8] E.D. Gaier, B.A. Eipper, R.E. Mains, Copper signaling in the mammalian nervous system: synaptic effects, J. Neurosci. Res. 91 (2013) 2–19, https://doi.org/10.1002/jnr.23143.
[9] M. Cendrowska-Pinkosz, M. Krauze, J. Juśkiewicz, B. Fotschki, K. Ognik, The influence of copper nanoparticles on Neurometabolism marker levels in the brain and intestine in a rat model, Int. J. Mol. Sci. 24 (2023) 11321, https://doi.org/10.3390/ijms241411321.
[10] M. Krauze, J. Juśkiewicz, B. Fotschki, M. Pinkosz, K. Ognik, Hippocampus and jejunum biochemical parameters related to physiological ageing of neurons in rats fed diets with copper nanoparticles and different fiber types, Ann. Anim. Sci. 0 (2024), https://doi.org/10.2478/aoas-2024-0019.
[11] S. Tian, J. Xu, X. Qiao, X. Zhang, S. Zhang, Y. Zhang, C. Xu, H. Wang, C. Fang, CuO nanoparticles for glioma treatment in vitro and in vivo, Sci. Rep. 14 (2024) 23229, https://doi.org/10.1038/s41598-024-74546-7.
[12] J.J. Kim, M.W. Jung, Neural circuits and mechanisms involved in Pavlovian fear conditioning: a critical review, Neurosci. Biobehav. Rev. 30 (2006) 188–202, https://doi.org/10.1016/j.neubiorev.2005.06.005.
[13] J.W. Kenney, I.C. Scott, S.A. Josselyn, P.W. Frankland, Contextual fear conditioning in zebrafish, Learn. Mem. 24 (2017) 516–523, https://doi.org/10.1101/lm.045690.117.
[14] A.K. Pribadi, S.H. Chalasani, Fear conditioning in invertebrates, Front. Behav. Neurosci. 16 (2022), https://doi.org/10.3389/fnbeh.2022.1008818.
[15] T.C.M. Bienvenu, C. Dejean, D. Jercog, B. Aouizerate, M. Lemoine, C. Herry, The advent of fear conditioning as an animal model of post-traumatic stress disorder: learning from the past to shape the future of PTSD research, Neuron 109 (2021) 2380–2397, https://doi.org/10.1016/j.neuron.2021.05.017.
[16] R.J. Fenster, L.A.M. Lebois, K.J. Ressler, J. Suh, Brain circuit dysfunction in post-traumatic stress disorder: from mouse to man, Nat. Rev. Neurosci. 19 (2018) 535–551, https://doi.org/10.1038/s41583-018-0039-7.
[17] K.J. Ressler, S. Berretta, V.Y. Bolshakov, I.M. Rosso, E.G. Meloni, S.L. Rauch, W. A. Carlezon, Post-traumatic stress disorder: clinical and translational neuroscience from cells to circuits, Nat. Rev. Neurol. 18 (2022) 273–288, https://doi.org/10.1038/s41582-022-00635-8.
[18] K.M. Myers, K.J. Ressler, M. Davis, Different mechanisms of fear extinction dependent on length of time since fear acquisition, Learn. Mem. 13 (2006) 216–223, https://doi.org/10.1101/lm.119806.
[19] J.-H. Cho, K. Deisseroth, V.Y. Bolshakov, Synaptic encoding of fear extinction in mPFC-amygdala circuits, Neuron 80 (2013) 1491–1507, https://doi.org/10.1016/j.neuron.2013.09.025.
[20] G.J. Quirk, E. Likhtik, J.G. Pelletier, D. Paré, Stimulation of medial prefrontal cortex decreases the responsiveness of central amygdala output neurons, J. Neurosci. 23 (2003) 8800–8807, https://doi.org/10.1523/JNEUROSCI.23-25-08800.2003.
[21] M.T. Sepulveda-Orengo, A.V. Lopez, O. Soler-Cedeño, J.T. Porter, Fear extinction induces mGluR5-mediated synaptic and intrinsic plasticity in Infralimbic neurons, J. Neurosci. 33 (2013) 7184–7193, https://doi.org/10.1523/JNEUROSCI.5198-12.2013.
[22] K. Ng, M. Pollock, A. Escobedo, B. Bachman, N. Miyazaki, E.L. Bartlett, S. Sangha, Suppressing fear in the presence of a safety cue requires infralimbic cortical signaling to central amygdala, Neuropsychopharmacology 49 (2024) 359–367, https://doi.org/10.1038/s41386-023-01598-0.
[23] D.W. Bloodgood, J.A. Sugam, A. Holmes, T.L. Kash, Fear extinction requires infralimbic cortex projections to the basolateral amygdala, Transl. Psychiatry 8 (2018) 1–11, https://doi.org/10.1038/s41398-018-0106-x.
[24] O. Perl, O. Duek, K.R. Kulkarni, C. Gordon, J.H. Krystal, I. Levy, I. Harpaz-Rotem, D. Schiller, Neural patterns differentiate traumatic from sad autobiographical

memories in PTSD, Nat. Neurosci. 26 (2023) 2226–2236, https://doi.org/10.1038/s41593-023-01483-5.
[25] A. Chen, Y. Kang, J. Liu, J. Wu, X. Feng, M. Wang, Y. Zhang, R. Wang, X. Lai, L. Shao, Improvement of synaptic plasticity by nanoparticles and the related mechanisms: applications and prospects, J. Control. Release 347 (2022) 143–163, https://doi.org/10.1016/j.jconrel.2022.04.049.
[26] L. An, S. Liu, Z. Yang, T. Zhang, Cognitive impairment in rats induced by nano-CuO and its possible mechanisms, Toxicol. Lett. 213 (2012) 220–227, https://doi.org/10.1016/j.toxlet.2012.07.007.
[27] E.I. Hassanen, M.A. Ibrahim, A.M. Hassan, S. Mehanna, S.H. Aljuaydi, M.Y. Issa, Neuropathological and cognitive effects induced by CuO-NPs in rats and trials for prevention using pomegranate juice, Neurochem. Res. 46 (2021) 1264–1279, https://doi.org/10.1007/s11064-021-03264-7.
[28] L.E. Maglio, J.A. Noriega-Prieto, I.B. Maroto, J. Martin-Cortecero, A. Muñoz-Callejas, M. Callejo-Móstoles, D. Fernández de Sevilla, IGF-1 facilitates extinction of conditioned fear, eLife 10 (2021) e67267, https://doi.org/10.7554/eLife.67267.
[29] D.C. Blanchard, R.J. Blanchard, Innate and conditioned reactions to threat in rats with amygdaloid lesions, J. Comp. Physiol. Psychol. 81 (1972) 281–290, https://doi.org/10.1037/h0033521.
[30] E.C. Nwanna, P.E. Imoisili, S.O. Bitire, T.-C. Jen, Biosynthesis and fabrication of copper oxide thin films as a P-type semiconductor for solar cell applications, Coatings 11 (2021) 1545, https://doi.org/10.3390/coatings11121545.
[31] H. Khelfaoui, C. Ibaceta-Gonzalez, M.C. Angulo, Functional myelin in cognition and neurodevelopmental disorders, Cell. Mol. Life Sci. 81 (2024) 181, https://doi.org/10.1007/s00018-024-05222-2.
[32] G. Sahu, R.W. Turner, The molecular basis for the calcium-dependent slow Afterhyperpolarization in CA1 hippocampal pyramidal neurons, Front. Physiol. 12 (2021), https://doi.org/10.3389/fphys.2021.759707.
[33] Y.J. Noh, R. Singh, J. Lee, J.K. Hyun, Copper oxide nanoparticles as a novel therapeutic approach for motor function recovery in spinal cord injury, IBRO Neurosci. Rep. 15 (2023) S618, https://doi.org/10.1016/j.ibneur.2023.08.1230.
[34] J. Radulovic, L.Y. Ren, C. Gao, N-methyl D-aspartate receptor subunit signaling in fear extinction, Psychopharmacology 236 (2019) 239–250, https://doi.org/10.1007/s00213-018-5022-5.
[35] K. Hu, Y. Liu, Q. Wang, Y. Xiong, Z. Guo, Z. Weng, Y. Liu, Y. Zhang, H. Wu, F. Ai, X. Wang, Copper nanoclusters based short-term memory “eraser,”, Chem. Eng. J. 463 (2023) 142366 https://doi.org/10.1016/j.cej.2023.142366.
[36] J. Morán, J. Yon, C. Henry, M.R. Kholghy, Approximating the van der Waals interaction potentials between agglomerates of nanoparticles, Adv. Powder Technol. 34 (2023) 104269, https://doi.org/10.1016/j.apt.2023.104269.
[37] H. Liu, W. Lai, X. Liu, H. Yang, Y. Fang, L. Tian, K. Li, H. Nie, W. Zhang, Y. Shi, L. Bian, S. Ding, J. Yan, B. Lin, Z. Xi, Exposure to copper oxide nanoparticles triggers oxidative stress and endoplasmic reticulum (ER)-stress induced toxicology and apoptosis in male rat liver and BRL-3A cell, J. Hazard. Mater. 401 (2021) 123349, https://doi.org/10.1016/j.jhazmat.2020.123349.
[38] S. Zia, A. Islam Aqib, A. Muneer, M. Fatima, K. Atta, T. Kausar, C.-N.F. Zaheer, I. Ahmad, M. Saeed, A. Shafique, Insights into nanoparticles-induced neurotoxicity and cope up strategies, Front. Neurosci. 17 (2023), https://doi.org/10.3389/fnins.2023.1127460.
[39] C. Distasi, F.A. Ruffinatti, M. Dionisi, S. Antoniotti, A. Gilardino, G. Croci, B. Riva, E. Bassino, G. Alberto, E. Castroflorio, D. Incarnato, E. Morandi, G. Martra, S. Oliviero, L. Munaron, D. Lovisolo, SiO2 nanoparticles modulate the electrical activity of neuroendocrine cells without exerting genomic effects, Sci. Rep. 8 (2018) 2760, https://doi.org/10.1038/s41598-018-21157-8.
[40] V. Castagnola, L. Deleye, A. Podestà, E. Jaho, F. Loiacono, D. Debellis, M. Trevisani, D.Z. Ciobanu, A. Armirotti, F. Pisani, E. Flahaut, E. Vazquez, M. Bramini, F. Cesca, F. Benfenati, Interactions of Graphene Oxide and Few-Layer Graphene with the Blood–Brain Barrier, Nano Lett. 23 (2023) 2981–2990, https://doi.org/10.1021/acs.nanolett.3c00377.
[41] D. Kim, J.M. Yoo, H. Hwang, J. Lee, S.H. Lee, S.P. Yun, M.J. Park, M. Lee, S. Choi, S.H. Kwon, S. Lee, S.-H. Kwon, S. Kim, Y.J. Park, M. Kinoshita, Y.-H. Lee, S. Shin, S. R. Paik, S.J. Lee, S. Lee, B.H. Hong, H.S. Ko, Graphene quantum dots prevent α-synucleinopathy in Parkinson’s disease, Nature Nanotech. 13 (2018) 812–818, https://doi.org/10.1038/s41565-018-0179-y.
[42] E. Santini, G.J. Quirk, J.T. Porter, Fear conditioning and extinction differentially modify the intrinsic excitability of Infralimbic neurons, J. Neurosci. 28 (2008) 4028–4036, https://doi.org/10.1523/JNEUROSCI.2623-07.2008.
[43] H.-S. Kim, H.-Y. Cho, G.J. Augustine, J.-H. Han, Selective control of fear expression by Optogenetic manipulation of Infralimbic cortex after extinction, Neuropsychopharmacology 41 (2016) 1261–1273, https://doi.org/10.1038/npp.2015.276.
[44] E. Santini, J.T. Porter, M-type potassium channels modulate the intrinsic excitability of Infralimbic neurons and regulate fear expression and extinction, J. Neurosci. 30 (2010) 12379–12386, https://doi.org/10.1523/JNEUROSCI.1295-10.2010.
[45] C. Stubbendorff, E. Hale, H.L.L. Day, J. Smith, G.S. Alvaro, C.H. Large, C. W. Stevenson, Pharmacological modulation of Kv3 voltage-gated potassium channels regulates fear discrimination and expression in a response-dependent manner, Prog. Neuro-Psychopharmacol. Biol. Psychiatry 127 (2023) 110829, https://doi.org/10.1016/j.pnpbp.2023.110829.
[46] C. Hansel, R. Yuste, Neural ensembles: role of intrinsic excitability and its plasticity, Front. Cell. Neurosci. 18 (2024), https://doi.org/10.3389/fncel.2024.1440588.
[47] H. Yousuf, V.L. Ehlers, M. Sehgal, C. Song, J.R. Moyer, Modulation of intrinsic excitability as a function of learning within the fear conditioning circuit, Neurobiol. Learn. Mem. 167 (2020) 107132, https://doi.org/10.1016/j.nlm.2019.107132.
[48] Oh, Learning and aging related changes in intrinsic neuronal excitability, Fronti. Ag.Neurosci. (2010), https://doi.org/10.3389/neuro.24.002.2010.
[49] E.D. Cui, B.W. Strowbridge, Selective attenuation of ether-a-go-go related K+ currents by endogenous acetylcholine reduces spike-frequency adaptation and network correlation, eLife 8 (2019) e44954, https://doi.org/10.7554/eLife.44954.
[50] N. Gu, K. Vervaeke, H. Hu, J.F. Storm, Kv7/KCNQ/M and HCN/h, but not KCa2/SK channels, contribute to the somatic medium after-hyperpolarization and excitability control in CA1 hippocampal pyramidal cells, J. Physiol. 566 (2005) 689–715, https://doi.org/10.1113/jphysiol.2005.086835.
[51] W.J. Spain, P.C. Schwindt, W.E. Crill, Anomalous rectification in neurons from cat sensorimotor cortex in vitro, J. Neurophysiol. 57 (1987) 1555–1576, https://doi.org/10.1152/jn.1987.57.5.1555.
[52] J.F. Storm, An after-hyperpolarization of medium duration in rat hippocampal pyramidal cells, J. Physiol. 409 (1989) 171–190, https://doi.org/10.1113/jphysiol.1989.sp017491.
[53] C. Distasi, M. Dionisi, F.A. Ruffinatti, A. Gilardino, R. Bardini, S. Antoniotti, F. Catalano, E. Bassino, L. Munaron, G. Martra, D. Lovisolo, The interaction of Sio2 nanoparticles with the neuronal cell membrane: activation of ionic channels and calcium influx, Nanomedicine 14 (2019) 575–594, https://doi.org/10.2217/nnm-2018-0256.
[54] D.E. Fontanez-Nuin, E. Santini, G.J. Quirk, J.T. Porter, Memory for fear extinction requires mGluR5-mediated activation of Infralimbic neurons, Cereb. Cortex 21 (2011) 727–735, https://doi.org/10.1093/cercor/bhq147.
[55] O. Soler-Cedeño, O. Torres-Rodríguez, F. Bernard, L. Maldonado, A. Hernández, J. T. Porter, Plasticity of NMDA receptors at ventral hippocampal synapses in the infralimbic cortex regulates cued fear, ENeuro 6 (2019) ENEURO.0354-18.2019, https://doi.org/10.1523/ENEURO.0354-18.2019.
[56] A. Burgos-Robles, I. Vidal-Gonzalez, E. Santini, G.J. Quirk, Consolidation of fear extinction requires NMDA receptor-dependent bursting in the ventromedial prefrontal cortex, Neuron 53 (2007) 871–880, https://doi.org/10.1016/j.neuron.2007.02.021.
[57] F. Sotres-Bayon, D.E.A. Bush, J.E. LeDoux, Acquisition of fear extinction requires activation of NR2B-containing NMDA receptors in the lateral amygdala, Neuropsychopharmacology 32 (2007) 1929–1940, https://doi.org/10.1038/sj.npp.1301316.
[58] S. Nakauchi, H. Su, K. Sumikawa, Nicotine and a positive allosteric modulator of m1 muscarinic receptor increase NMDA/AMPA ratio in the hippocampus and medial prefrontal cortex, Neuropharmacology 262 (2025) 110213, https://doi.org/10.1016/j.neuropharm.2024.110213.